Surface-enhanced Raman scattering-based immunoassay for severe acute respiratory syndrome coronavirus 2

Hyunjung Cha [a], Hyeran Kim [a], Younju Joung [b], Hyunju Kang [a], Jeong Moon [a,c], Hyowon Jang [a], Sohyun Park [b], Hyung-Jun Kwon [d], In-Chul Lee [d], Sunjoo Kim [e], Dongeun Yong [f], Sun-Woo Yoon [a], Sung-Gyu Park [g], Kyeonghye Guk [a], Eun-Kyung Lim [a,h], Hyun Gyu Park [c], Jaebum Choo [b,**], Juyeon Jung [a,***], Taejoon Kang [a,*]

[a] Bionanotechnology Research Center, Korea Research Institute of Bioscience and Biotechnology (KRIBB), Daejeon, 34141, Republic of Korea
[b] Department of Chemistry, Chung-Ang University, Seoul, 06974, Republic of Korea
[c] Department of Chemical and Biomolecular Engineering, Korea Advanced Institute of Science and Technology (KAIST), Daejeon, 34141, Republic of Korea
[d] Functional Biomaterial Research Center, Korea Research Institute of Bioscience and Biotechnology (KRIBB), Jeongeup, 56212, Republic of Korea
[e] Department of Laboratory Medicine, Gyeongsang National University College of Medicine, Jinju, 52828, Republic of Korea
[f] Department of Laboratory Medicine and Research Institute of Bacterial Resistance, Yonsei University College of Medicine, Seoul, 03722, Republic of Korea
[g] Nano-Bio Convergence Department, Korea Institute of Materials Science (KIMS), Changwon, 51508, Republic of Korea
[h] Department of Nanobiotechnology, KRIBB School of Biotechnology, University of Science and Technology (UST), Daejeon, 34113, Republic of Korea

ABSTRACT

Severe acute respiratory syndrome coronavirus 2 (SARS-CoV-2) has affected humans worldwide for over a year now. Although various tests have been developed for the detection of SARS-CoV-2, advanced sensing methods are required for the diagnosis, screening, and surveillance of coronavirus disease 2019 (COVID-19). Here, we report a surface-enhanced Raman scattering (SERS)-based immunoassay involving an antibody pair, SERS-active hollow Au nanoparticles (NPs), and magnetic beads for the detection of SARS-CoV-2. The selected antibody pair against the SARS-CoV-2 antigen, along with the magnetic beads, facilitates the accurate direct detection of the virus. The hollow Au NPs exhibit strong, reproducible SERS signals, allowing sensitive quantitative detection of SARS-CoV-2. This assay had detection limits of 2.56 fg/mL for the SARS-CoV-2 antigen and 3.4 plaque-forming units/mL for the SARS-CoV-2 lysates. Furthermore, it facilitated the identification of SARS-CoV-2 in human nasopharyngeal aspirates and diagnosis of COVID-19 within 30 min using a portable Raman device. Thus, this assay can be potentially used for the diagnosis and prevention of COVID-19.

1. Introduction

Coronavirus disease 2019 (COVID-19), caused by severe respiratory syndrome coronavirus 2 (SARS-CoV-2), was first reported in December 2019, and it soon resulted in a pandemic in March 2020 (Lu et al., 2020). Currently, over 240 million infections and 4.8 million deaths due to COVID-19 have been reported worldwide (World Health Organization, 2021). Although several types of SARS-CoV-2 vaccines have been developed and administered, new SARS-CoV-2 infections are still detected worldwide (Richman, 2021).

Soon after the emergence of SARS-CoV-2, the virus was genetically

analyzed to facilitate the development of diagnostic methods for COVID-19 (Khan et al., 2020). Therefore, polymerase chain reaction (PCR)-based approaches have been widely used for the detection of viral RNA (Corman et al., 2020). In addition, several types of antigen tests, such as the sandwich-type immunofluorescence strip assay (Zhang et al., 2020), colorimetric lateral flow assay (Grant et al., 2020), field-effect transistor sensors (Seo et al., 2020), microfluidic enzyme-linked immunosorbent assay (ELISA) (Lin et al., 2020), surface plasmon resonance sensors (Huang et al., 2021), and others (Cennamo et al., 2021; Eissa et al., 2021), have been developed for detection of SARS-CoV-2. However, there is still an increasing demand for public health tools for

diagnosis, screening, and surveillance (Mina and Andersen, 2021); thus, it is important to develop state-of-the-art methods for the detection of SARS-CoV-2.

Surface-enhanced Raman scattering (SERS) is a powerful analytical technique that can generate molecular fingerprint spectra with single-molecule sensitivity that is insensitive to quenching (Kahraman et al., 2017). SERS-based sensing methods have been limited because of the low reproducibility caused by the fluctuations in the SERS signals (Kang et al., 2010). However, recent advancements in SERS have led to the development of sophisticated sensing methods that facilitate precise analysis and generation of high-quality SERS-active nanostructures (Hwang et al., 2019; Shin et al., 2018). In particular for the combat with COVID-19, SERS technology has not only exhibited less time-cost advantages than PCR for detection SARS-CoV-2 and antibodies, but also exhibited more advantages such as identifying infectiousness of SARS-CoV-2 (Peng et al., 2021a,b; Zhang et al., 2021; Wu et al., 2022; Yang et al., 2021; Yu et al., 2021; Srivastav et al., 2021; Sanchez et al., 2021; Payne et al., 2021; Liu et al., 2021; Li et al., 2021; Huang et al., 2021; Gao et al., 2021; Chen et al., 2021; Chen et al., 2021, 2021; Huang et al., 2021, 2021; Pramanik et al., 2021; Zavyalova et al., 2021).

Here, we report a magnetically assisted SERS immunoassay for the detection of SARS-CoV-2. An antibody pair consisting of detection and reporter antibodies, with binding affinities (K_d) of 0.66 nM and 0.69 nM, respectively, to the SARS-CoV-2 antigen, was selected using a phage display library. For the SERS-based assay, the magnetic beads were modified with the detection antibody, and hollow Au nanoparticles (NPs) were synthesized and modified with the reporter antibody and Raman dye. In the presence of SARS-CoV-2, the hollow Au NPs undergo immunoreactions and associate with the magnetic beads, thus generating strong SERS signals. This assay can detect the SARS-CoV-2 antigen even at concentrations as low as 2.56 fg/mL and the SARS-CoV-2 lysates at 3.4 plaque-forming unit (PFU)/mL. In addition, it can effectively detect SARS-CoV-2 in human nasopharyngeal aspirates and thus help in the diagnosis of COVID-19 patients. The present assay exhibits distinct merits compared with previous immunoassays. First, the newly discovered antibody pair facilitates the specific recognition of SARS-CoV-2. The antibody pair might be useful to the various immunological devices for COVID-19 diagnosis. Second, the adoption of SERS technique enables the sensitive and quantitative detection of the virus, being beneficial than the conventional lateral flow assays. Third, this SERS-based method will be helpful for the on-site detection of SARS-CoV-2 using a portable Raman system. SERS-based assays for the direct detection of SARS-CoV-2 in clinical samples have not been developed so far. Considering the recent advancements in SERS, such assays would greatly help in the diagnosis of COVID-19 patients.

2. Materials and methods

2.1. Materials

Gold (III) chloride trihydrate (HAuCl$_4$·3H$_2$O), cobalt (II) chloride hexahydrate (CoCl$_2$·6H$_2$O), sodium borohydride (NaBH$_4$), trisodium citrate dihydrate (HOC(COONa)(CH$_2$COONa)$_2$·3H$_2$O), tosyl phenyl-alanyl chloromethyl ketone (TPCK) trypsin, bovine serum albumin (BSA), 2-(N-morpholino) ethane sulfonic acid (MES), 1-ethyl-3-(3-dimethylaminopropyl) carbodiimide (EDC), N-hydroxysuccinimide (NHS), ethanol, tetrahydrofuran (THF), and isopropyl β-D-1-thiogalactopyr-anoside were purchased from Sigma-Aldrich (MO, USA). Phosphate buffered saline (PBS) (10X, pH 7.4) and carboxylic acid-activated magnetic beads (Dynabeads MyOne) were purchased from Invitrogen (OR, USA). Dulbecco's modified Eagle medium (DMEM) and antibiotic-antimycotic were purchased from Thermo Fisher Scientific (MA, USA). Malachite green isothiocyanate (MGITC) was purchased from Setareh Biotech (OR, USA). Tris(2-carboxyethyl) phosphine (TCEP) was purchased from LPS Solution (Korea). Ethylenediaminetetraacetic acid (EDTA) solution was purchased from Dyne Bio (Korea). SARS-CoV-2

antigen (nucleocapsid protein), SARS-CoV-2 S-protein, influenza M1, neuraminidase (N), hemagglutinin (HA) proteins, respiratory syncytial virus fusion (F) protein, human CoV 229E, influenza A/CA/07/2009 (pH1N1), influenza A/Brisbane/10/2007 (H3N2), influenza A/aquatic bird/Korea/w351/2008 (H5N2), and influenza B/Victoria/Brisbane/60/2008 (IBV) were provided by the BioNano Health Guard Research Center (H-GUARD) of Korea. SARS-CoV-2 (BetaCoV/Korea/KCDC03/2020) was obtained from the National Culture Collection for Pathogens, which is operated by the Korea National Institute of Health.

2.2. Screening of antibodies

The screening of the antibody pair was carried out using a large Fab phage display library (5×10^{11}) in KRIBB (Guk et al., 2020). Briefly, 96-well microplates were coated with 100 ng of SARS-CoV-2 antigen, incubated at 37 °C for 1 h, washed with PBS, and then blocked with 4% skim milk in PBS at 37 °C for 1 h. The antibody library phages were further incubated with the antigen-coated plates at 37 °C for 1 h. The unbound phage was washed with 0.05% Tween 20 in PBS (PBST), and the bound phages were eluted with 0.1 M glycine-HCl (pH 2.2) and neutralized with 2 M Tris base. The TG1 cells were first infected with the eluted phages and then superinfected with helper phages (VCSM13). The resulting phages were subjected to additional rounds of panning. Individual TG1 colonies were randomly isolated from the output of the third round of panning and cultured in Superbroth medium containing 100 μg/mL ampicillin until an optical density of 0.5 at 600 nm was obtained. Isopropyl β-D-1-thiogalactopyranoside (final concentration = 1 mM) was then added to the culture and incubated overnight at 30 °C to induce Fab expression. The clone-cultured supernatants were used for ELISA to screen for the antigen-specific antibodies. Goat F(ab')2 anti-human IgG (Fab')2-HRP antibody (1:1000, Abcam, UK) was used for the colorimetric detection of the bound clones using a 3,3′5,5′-tet-ramethylbenzimidine (TMB) substrate (BD Bioscience, NJ, USA).

2.3. ELISA

Various concentrations (10^{-13}–10^{-5} M) of the SARS-CoV-2 antigen were combined with an antibody (2 μg/mL) in PBS containing 0.1% BSA and pre-incubated at 37 °C for 2 h. The antigen-antibody mixtures were transferred to separate wells of a 96-well microplate coated with 100 ng of antigen, and the bound antibody was then detected via indirect ELISA. The K_d of antibody to antigen was calculated using a Klotz plot.

For sandwich ELISA, the microplates coated with 100 ng of the detection antibody in PBS were incubated with 100 ng of the SARS-CoV-2 antigen and 100 ng of the respective proteins at 37 °C for 2 h. Next, the plates were washed with PBST, and 100 ng of the reporter antibody was added and incubated at 37 °C for 1 h. For the colorimetric detection of the bound reporter antibody, a goat anti-human IgG-HRP antibody (1:3000, Pierce, MA, USA) and a TMB substrate (BD Bioscience) were used.

2.4. Dot-blot test

Each virus (2×10^2 TCID$_{50}$/dot) was blotted onto the nitrocellulose (NC) membrane and air-dried. The membrane was then incubated with the detection or reporter antibodies (1 μg/mL) in BSA/PBST for 2 h at 37 °C. The bound antibody was detected using a goat anti-human IgG-HRP antibody (1:3000, Pierce) and enhanced chemiluminescent reagent (Thermo Fisher Scientific) using a ChemiDoc MD gel documentation system (Bio-Rad, CA, USA).

2.5. Synthesis of hollow Au NPs

Deionized water (100 mL) was placed in a three-neck round-bottomed flask with 1 mL of 0.1 M sodium citrate solution (0.1 M). The solution was deoxygenated with N$_2$ gas for 50 min. Next, 140 μL of

NaBH$_4$ (1.0 M) and 100 μL of CoCl$_2$ solution (0.4 M) were added to the solution and reacted for 45 min under N$_2$ gas flow. A total of 500 μL of HAuCl$_4$ solution (0.1 M) was added to the solution through 10 separate additions of 50 μL aliquots at intervals of 80 s after the reaction was complete. Furthermore, the resultant solution was exposed to ambient conditions after reaction for 40 min. Lastly, the synthesized hollow Au NPs were centrifuged at 1100 × g for 20 min at 25 °C and resuspended in PBS before further use.

2.6. Detection of SARS-CoV-2

To prepare the detection antibody-conjugated magnetic beads, 1 mg of magnetic beads was washed twice with MES buffer (25 mM, pH 6). Next, 50 μL of EDC solution (50 mg/mL) and 50 μL of NHS solution (50 mg/mL) were sequentially added to the magnetic beads and reacted with slow tilt rotation for 30 min. EDC/NHS coupling has been widely used for antibody conjugation (Guk et al., 2020). After the reaction, the beads were separated using a magnet and washed twice with 25 mM MES buffer. Next, 10 μg of the detection antibody was added to the beads suspended in 100 μL of MES buffer (25 mM), and the resultant solution was incubated for 4 h at 25 °C. After incubation, the excess antibody was eliminated by washing thrice with PBS buffer. The unreacted surfaces of the beads were blocked by incubating with BSA solution (1%) for 1 h and washing with PBS. Lastly, the detection antibody-conjugated magnetic beads were resuspended in PBS buffer (final concentration = 10 mg/mL).

Furthermore, to prepare the reporter antibody-conjugated hollow Au NPs with MGITC, 3 mL of the synthesized hollow Au NP solution was centrifuged at 2500 × g for 20 min and resuspended in 10 mL PBS buffer (10 mM). Then, 8 μL of MGITC solution (100 mM in ethanol) was added to the hollow Au NP solution and incubated for 45 min with gentle shaking. The MGITC-modified Au NPs were centrifuged at 13,000 × g for 10 min and resuspended in 1 mL of PBS buffer (10 mM). During the MGITC coating reaction, 5 μL of HS-(CH$_2$)$_{10}$-NHS solution (100 μM in THF) was mixed with 100 μL of the reporter antibody solution (10 μg/mL in PBS) and incubated for 45 min at 25 °C with orbital shaking. Then, 50 μL of the resultant antibody solution was added to the MGITC-modified hollow Au NP solution and further incubated for 1 h at 25 °C. After incubation, the reporter antibody-conjugated hollow Au NPs with MGITC were centrifuged at 13,000 × g for 10 min and resuspended in 500 μL of PBS (10 mM). Both MGITC and reporter antibody were conjugated to hollow Au NPs through Au–S bonding.

For the detection of the SARS-CoV-2 antigen, 100 μL of sample solution, 50 μL of detection antibody-conjugated magnetic bead solution, and 50 μL of reporter antibody-conjugated hollow Au NP solution were mixed in a reaction tube and incubated for 2 h at 25 °C. The beads were then separated using an external magnet for 30 s and washed with PBS buffer. The SERS signals from the magnetically collected beads were measured for 30 s.

For the preparation of the SARS-CoV-2 culture, the procured virus was propagated in Vero cells (ATCC No. CCL-81) in DMEM containing 1% antibiotic-antimycotic and TPCK trypsin without fetal bovine serum at 37 °C under 5% CO$_2$ for 72 h. Infectious virus titers were determined by 50% tissue culture infective dose (TCID$_{50}$) in the confluent cells cultured in 96-well microplates. All experiments using SARS-CoV-2 were performed at a Korea Centers for Disease Control and Prevention (KCDC)-approved BL-3 facility of KRIBB in accordance with institutional biosafety guidelines. Influenza virus titers were determined using a one-step real-time PCR kit (Promega, WI, USA) in accordance with the manufacturer's instructions.

For the detection of SARS-CoV-2, 90 μL of the viral sample was treated with 10 μL of TCEP/EDTA (final concentrations of 100 and 1 mM, respectively) and heated at 50 °C for 5 min and 64 °C for 5 min. This step was performed for the lysis of SARS-CoV-2. Next, 100 μL of sample solution, 50 μL of detection antibody-conjugated magnetic bead solution, and 50 μL of reporter antibody-conjugated hollow Au NP

solution were mixed in a reaction tube and incubated for 2 h at 25 °C. The beads were then separated using an external magnet for 30 s and washed with PBS buffer. The SERS signals from the magnetically collected beads were measured for 30 s.

2.7. Diagnosis of COVID-19 patients

Nasopharyngeal aspirate samples from patients were collected using flocked nasopharyngeal swabs and placed in viral transport media (VTM, Copan Diagnostics Inc., CA, USA). All the patients were negatively diagnosed for COVID-19, and the patient samples were stored at −70 °C until further use. The protocol for this retrospective study was reviewed and approved by the Institutional Review Board (IRB) of the Yonsei University Health Service Center, Severance Hospital, Seoul, Korea (IRB approval number: 4-2020-0465). For the detection of SARS-CoV-2 in the human nasopharyngeal aspirates, 45 μL of SARS-CoV-2-spiked nasopharyngeal aspirate sample was treated with 5 μL of TCEP/EDTA (final concentrations of 100 and 1 mM, respectively) and heated at 50 °C for 5 min followed by 64 °C for 5 min. Next, 50 μL of sample solution, 25 μL of detection antibody-conjugated magnetic bead solution, and 25 μL of reporter antibody-conjugated hollow Au NP solution were mixed in a reaction tube and incubated at 25 °C for 30 min. The beads were then separated using an external magnet for 30 s and washed with PBS buffer. Lastly, the SERS signals from the magnetically collected beads were measured for 30 s.

Clinical samples from COVID-19 patients were collected and placed in VTM and stored at −70 °C until use. The protocol for this retrospective study was reviewed and approved by the IRB of Gyeongsang National University College of Medicine, Jinju, Korea (IRB approval number: 2020-10-002). For the diagnosis of COVID-19 patients, 40 μL of the clinical sample solution, 20 μL of detection antibody-conjugated magnetic bead solution, and 20 μL of reporter antibody-conjugated hollow Au NP solution were mixed in a reaction tube and incubated at 25 °C for 25 min. The beads were then separated using an external magnet for 30 s and washed with PBS buffer. Lastly, the SERS signals from the magnetically collected beads were measured using a portable Raman device.

PCR analysis of the clinical samples was performed using the reference primers and probes targeting the envelope and RNA-dependent RNA polymerase (RdRp) genes according to World Health Organization guidelines (Álvarez-Díaz et al., 2020). Total viral RNA was purified using the QIAamp Viral RNA Mini Kit (Qiagen, Germany) according to the manufacturer's instructions. The one-step real-time reverse transcription-quantitative PCR (RT-qPCR) reaction mixture consisted of 5 μL of the RNA template, 10 μL 2× reaction buffer supplemented with the SensiFAST Probe No-ROX One-Step Mix (Bioline, TN, USA), 0.2 μL reverse transcriptase (Bioline), 0.4 μL RNase inhibitor (Bioline), 1 μL each of the forward and reverse primers (10 pmol), 1 μL of each probe (5 μM), and RNase-free water to adjust the final volume to 20 μL. The cycling conditions used were as follows: initial at 45 °C for 15 min and 95 °C for 10 min for the reverse transcription step, followed by 40 cycles at 95 °C for 5 s and 58 °C for 30 s.

2.8. Instrumentation

SERS measurements were carried out using a micro-Raman system based on an Olympus BX41 microscope (Nanobase, Korea). The excitation source was a He−Ne laser operating at λ = 633 nm, and the laser spot was focused on the sample through a 20× objective lens. The SERS signals were recorded using a thermodynamically cooled electron-multiplying charge-coupled device (Andor, UK) mounted on a spectrometer with 1200 groove/mm grating. A portable Raman device was purchased from Metrohm (Switzerland). A diode laser operating at λ = 638 nm was used as the excitation source. The baseline correction of Raman spectra was performed using NanoSpectrum XperRF C series software (Nanobase, Korea). The spectral analysis was performed using

Origin Pro V8 software (OriginLab Corporation, MA, USA). Transmission electron microscopy (TEM) images were obtained using a Tecnai G2 F30 S-Twin microscope (OR, USA) operated at 300 kV. Absorbance spectra were obtained using Cytation 5 (BioTek, VT, USA), and dynamic light scattering (DLS) data were acquired using a Nano-ZS90 (Malvern, UK). RT-qPCR assays were performed using the Light-Cycler 96 instrument and analysis software (Roche, Switzerland).

3. Results

3.1. Magnetically assisted SERS immunoassay for SARS-CoV-2

Several SERS-based immunoassays have been developed for the diagnosis of various viral diseases such as flu (Sun et al., 2017), severe acute respiratory syndrome (SARS) (Guo et al., 2017), middle east respiratory syndrome, hepatitis (Saviñon-Flores et al., 2021), and acquired immune deficiency syndrome (Kamińska et al., 2017; Yadav et al., 2021), which have facilitated the sensitive and selective detection of the viruses. In this study, we developed a magnetically assisted SERS immunoassay for the detection of SARS-CoV-2 (Fig. 1). First, the detection antibody was conjugated with the carboxylic acid-functionalized magnetic beads through EDC/NHS coupling, and the reporter antibody and MGITC were conjugated with the hollow Au NPs through Au–S bonding. The detection antibody-conjugated magnetic beads, reporter antibody-conjugated hollow Au NPs with MGITC, and sample solution were mixed in a reaction tube for the assay. After incubation, the magnetic beads were concentrated using an external magnet, and SERS measurement was carried out. In the presence of SARS-CoV-2, the hollow Au NPs are assembled with the magnetic beads through immunoreactions between the antibody pairs and the viruses in the sample. Thus, strong SERS signals of MGITC can be observed in the presence of SARS-CoV-2 because the hollow Au NPs carry MGITC, a well-known Raman dye that generates a distinct spectrum (Eom et al., 2019a,b). However, in the absence of the virus, the magnetic beads are collected by the magnet and lead to negligible signals.

The current assay has the following properties beneficial for the accurate, rapid, and easy detection of SARS-CoV-2: (1) the developed antibody pair enables the specific recognition of SARS-CoV-2; (2) the hollow Au NPs provide several SERS hot spots, thus enhancing the sensitivity for detection of the virus; and (3) the magnetically assisted assay facilitates the efficient separation of SARS-CoV-2 from complex
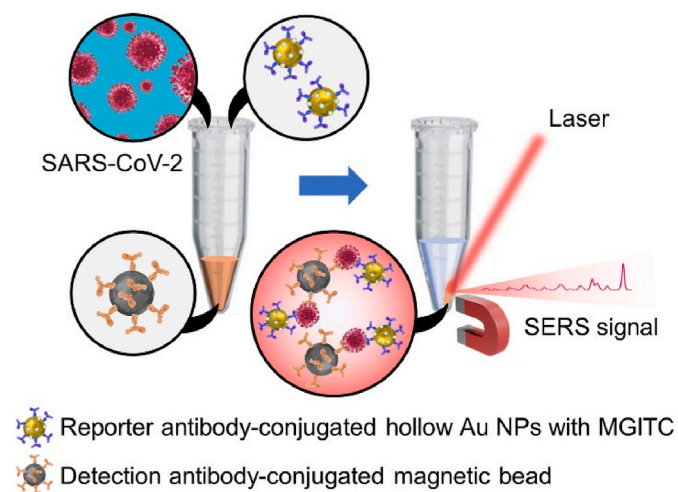

Fig. 1. Schematic illustration of the magnetically assisted SERS immunoassay for SARS-CoV-2. Detection antibody-conjugated magnetic beads, reporter antibody-conjugated hollow Au NPs with MGITC, and sample solution are mixed in the reaction tube. After incubation, the magnetic beads are concentrated using a magnet and SERS signals are measured.

clinical samples and enables direct identification of the virus from the samples of COVID-19 patients.

Antibodies, especially monoclonal antibodies, are commonly used biological receptors for the detection of biochemical molecules (Forthal, 2014) due to their high affinity and consistency, low cross-reactivity, overall stability, and ease of mass production (Mahmuda et al., 2017). Therefore, it is crucial to develop antibodies against SARS-CoV-2 for the development of efficient COVID-19 immunoassays. We generated two monoclonal antibodies against the SARS-CoV-2 antigen using a large human fragment antigen-binding (Fab) phage display library. The antibody candidates were screened using a biopanning process, and two clones that strongly bind to the antigen were selected. Next, the antibodies were converted from the library-selected Fab forms to the full immunoglobulin G (IgG) forms. Fig. 2 a and b show the amino acid sequences of the detection and reporter antibodies, respectively. The complementarity determining regions (CDRs) of the antibodies are marked in red. Using competitive ELISA, the K_d of the detection and reporter antibodies was found to be 0.66 nM and 0.69 nM, respectively (Fig. 2 c and d). The high binding affinities of the antibodies facilitate the sensitive detection of the SARS-CoV-2 antigen. In addition, we used sandwich ELISA for the antigen using the developed antibody pair (Fig. S1) and found that the developed antibody pair recognizes the antigen selectively and is thus suitable for the development of the magnetically assisted SERS immunoassay for SARS-CoV-2.

The selected detection and reporter antibodies were further characterized using dot-blot tests by spotting SARS-CoV-2, human coronavirus (CoV) 229E, and influenza A virus (pH1N1) on a nitrocellulose membrane. As shown in Fig. 2e, the dark spots were observed only in the presence of SARS-CoV-2, thus verifying that the screened antibodies specifically recognize SARS-CoV-2. These data are particularly critical considering that lack of specificity due to false-positive outcomes from the antigens well-conserved among different CoV species is one of the major challenges in the currently used immunodiagnostic approaches.

Furthermore, for the successful development of immunoassays, it is important to precisely combine high-performance bioreceptors with immune substrates and/or immunoprobes (Hwang et al., 2019). In this magnetically assisted SERS immunoassay, the detection antibody-conjugated magnetic beads were prepared easily in a routine manner and employed as immune substrates. Fig. 3a is the TEM image of the detection antibody-conjugated magnetic beads. Hollow Au NPs were synthesized by galvanic exchange of Co NPs for the preparation of the immunoprobes (Choi et al., 2020). The TEM image of the hollow Au NPs shows their uniform morphology (Fig. 3b), and the high magnification image (inset of Fig. 3b) clearly shows the hollow structure of the Au NPs. We measured the DLS of the hollow Au NPs and obtained an average diameter of 55.7 nm (blue bars in Fig. 3c), conforming with the TEM image. After synthesis, the reporter antibody and MGITC were conjugated to the hollow Au NPs, and thus their diameter increased to 68.5 nm (red bars in Fig. 3c). The estimated numbers of reporter antibody and MGITC are 10 and 4000 molecules/hollow Au NPs, respectively (Eom et al., 2019a,b). The UV/vis spectra further confirmed the successful modification of the antibodies using the hollow Au NPs. As shown in Fig. 3d, the peak of the reporter antibody-conjugated NPs was slightly more red-shifted than that of the bare NPs. Lastly, the SERS spectrum was measured using the reporter antibody-conjugated hollow Au NPs with MGITC (Fig. 3e). The main peaks of MGTIC are assigned as in-plane C–H bend and benzene v_9 mode for 1170 cm^{-1}, N–C stretch and NR$_2$ bend for 1220 cm^{-1}, in-plane C–H and C–C–H for 1295 cm^{-1}, stretch/bend of in-plane ring for 1590 cm^{-1}, and stretch of C–C and N-phenyl ring for 1620 cm^{-1} (Schechinger et al., 2019). The SERS hotspots can be generated on the pinholes of the hollow Au NPs, and thus, individual NPs show strong electromagnetic field enhancement and SERS signals (Choi et al., 2020). This indicates that the prepared hollow Au NP probes can be excellent SERS-active immunoprobes for the detection of SARS-CoV-2.
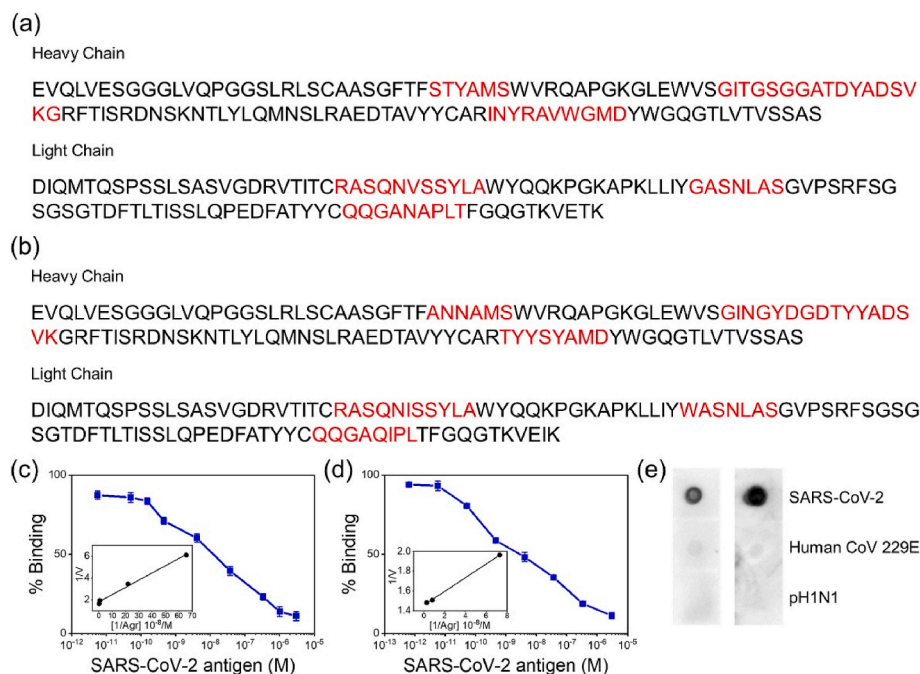
(a)

Heavy Chain

EVQLVESGGGLVQPGGSLRLSCAASGFTF STYAMS WVRQAPGKGLEWVS GITGSGGATDYADSV
KG RFTISRDNSKNTLYLQMNSLRAEDTAVYYCAR INYRAVWGMD YWGQGTLVTVSSAS

Light Chain

DIQMTQSPSSLSASVGDRVTITC RASQNVSSYLA WYQQKPGKAPKLLIY GASNLAS GVPSRFSG
SGSGTDFTLTISSLQPEDFATYYC QQGANAPLT FGQGTKVETK

(b)

Heavy Chain

EVQLVESGGGLVQPGGSLRLSCAASGFTF ANNAMS WVRQAPGKGLEWVS GINGYDGDTYYADS
VK GRFTISRDNSKNTLYLQMNSLRAEDTAVYYCAR TYYSYAMD YWGQGTLVTVSSAS

Light Chain

DIQMTQSPSSLSASVGDRVTITC RASQNISSYLA WYQQKPGKAPKLLIY WASNLAS GVPSRFSGSG
SGTDFTLTISSLQPEDFATYYC QQGAQIPL TFGQGTKVEIK

Fig. 2. (a, b) Amino acid sequences of the (a) detection and (b) reporter antibodies. CDRs of the antibodies are marked in red. (c, d) Binding affinities of the (c) detection and (d) reporter antibodies to SARS-CoV-2 antigen measured by competitive ELISA. Insets represent the Klotz plots. Data represent the average ± standard deviation from 3 measurements. (e) Dot-blot images obtained after the interaction of the detection (left) and reporter (right) antibodies with the viruses (SARS-CoV-2, Human CoV 229E, and pH1N1). (For interpretation of the references to color in this figure legend, the reader is referred to the Web version of this article.)
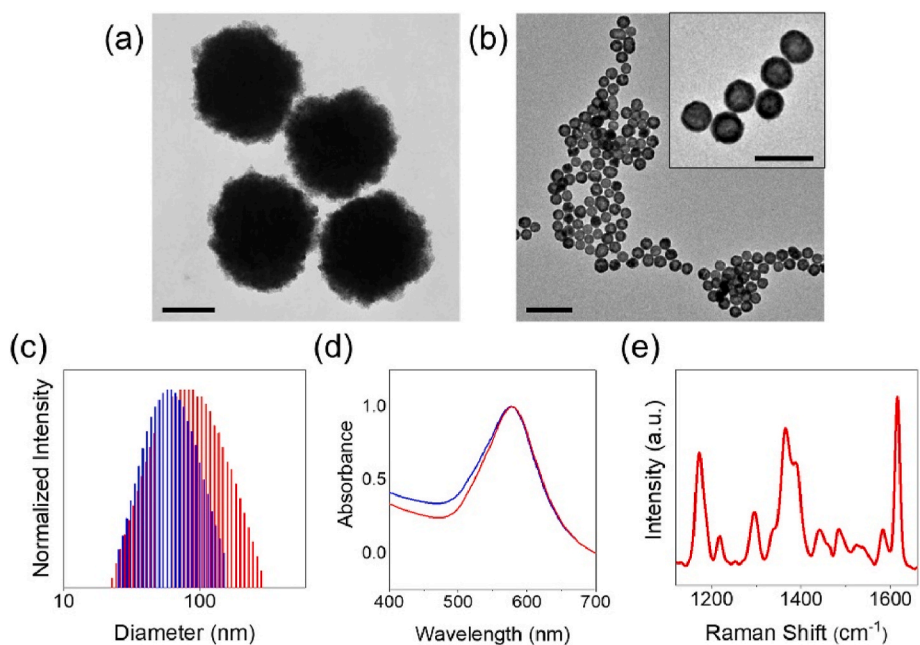

Fig. 3. (a) TEM image of the detection antibody-conjugated magnetic beads. Scale bar denotes 500 nm. (b) TEM image of the hollow Au NPs. Scale bar denotes 200 nm. Inset shows a magnified TEM image of the hollow Au NPs. Scale bar denotes 100 nm. (c) DLS distribution of the bare hollow Au NPs (blue bars) and reporter antibody-conjugated hollow Au NPs with MGITC (red bars). (d) UV–vis spectra of the bare hollow Au NPs (blue) and reporter antibody-conjugated hollow Au NPs with MGITC (red). (e) SERS spectrum of the reporter antibody-conjugated hollow Au NPs with MGITC. (For interpretation of the references to color in this figure legend, the reader is referred to the Web version of this article.)

3.2. Detection of SARS-CoV-2

Next, we tried to detect the antigen of SARS-CoV-2, as shown in Fig. 4a. Briefly, the prepared magnetic beads and hollow Au NPs were mixed with a sample solution, incubated in a reaction tube, and separated using an external magnet. Fig. 4b is a TEM image of the hollow Au NP-assembled magnetic beads after the detection of the SARS-CoV-2 antigen. The hollow Au NPs are attached to the magnetic beads through a sandwich formation of detection antibody-antigen-reporter antibody. The SERS spectra were then measured from the collected magnetic beads to precisely detect the antigen. Fig. 4c indicates the SERS spectra of MGITC obtained from the collected beads with the increasing concentration of the antigen. Negligible signals were

observed in the blank sample, whereas with the increased protein concentration, the SERS signals became increasingly distinct. For the quantitative analysis, the 1170 cm^{-1} band intensity was plotted as a function of protein concentration (Fig. 4d). Data represent average ± standard deviation from 10 measurements (Fig. S2). The band intensity increased linearly from 10 fg/mL to 100 pg/mL, and the fitted line $y = 406x + 1352$ has an R^2 value of 0.98. The limit of detection (LOD) was 2.56 fg/mL calculated based on LOD = 3sd/m, where sd is the standard deviation of 1170 cm^{-1} SERS intensity for the blank samples, and m is the slope of the linearly fitted curve. In this assay, the antibody-conjugated magnetic beads act as immune substrates and the reporter antibody-conjugated hollow Au NPs with MGITC as immunoprobes. Since the SERS signals were contributed to the immunoprobes with
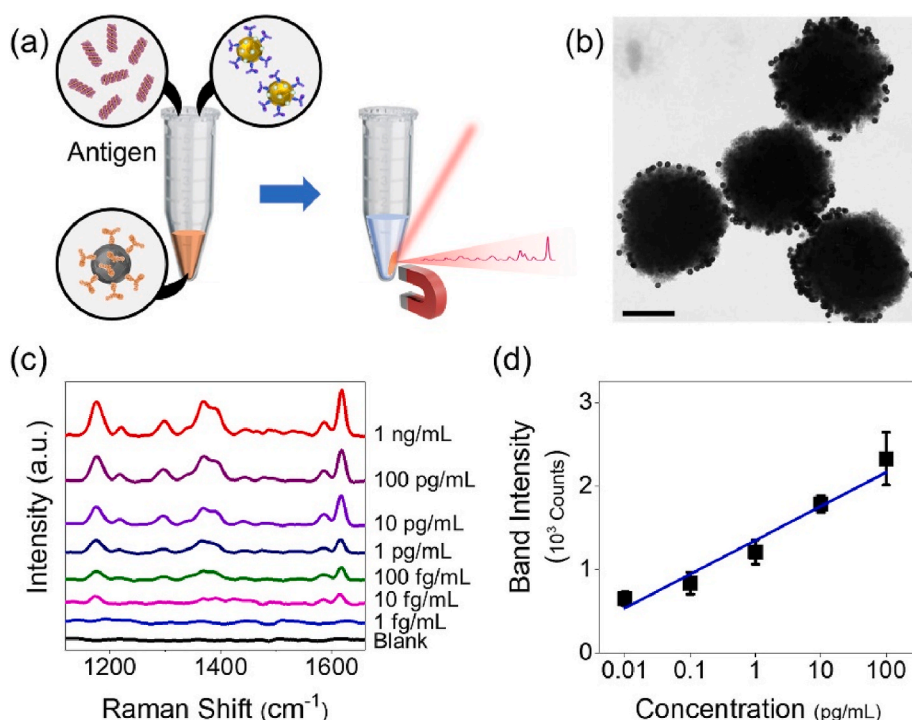
Fig. 4. (a) Schematic illustration of the magnetically assisted SERS immunoassay for the SARS-CoV-2 antigen. (b) TEM image of hollow Au NP-assembled magnetic beads after detection of the SARS-CoV-2 antigen. (c) SERS spectra of MGITC measured from the hollow Au NP-assembled magnetic beads after the detection of the SARS-CoV-2 antigen (0–1 ng/mL). (d) A plot of 1170 cm^{-1} band intensity as a function of the SARS-CoV-2 antigen concentration. The blue line is linearly fitted. Data represent average ± standard deviation from 10 measurements. (For interpretation of the references to color in this figure legend, the reader is referred to the Web version of this article.)

MGITC, the linear relationship between the signals and protein concentration could be obtained. The high antigen affinity of the antibodies, strong SERS enhancement of the hollow Au NPs, and magnetic separation synergistically contributed to the sensitivity of detection of the SARS-CoV-2 antigen.

Thereafter, we tried to detect SARS-CoV-2 using the magnetically assisted SERS immunoassay. SARS-CoV-2 was provided by the Korea National Institute of Health. For the detection, the virus was carefully cultured in the biosafety level 3 laboratory of KRIBB and heated with a lysis buffer. The SARS-CoV-2 lysates were mixed with the detection antibody-conjugated magnetic beads and reporter antibody-conjugated hollow Au NPs with MGITC as shown in Fig. 5a. After incubation, the magnetic beads were collected using an external magnet, and the SERS spectra were measured. Fig. 5b shows the SERS spectra of MGITC measured from the collected samples. The SERS signals increased with the increasing concentration of SARS-CoV-2. The SERS signals obtained in the presence of only a few PFU/mL of SARS-CoV-2 were more distinguishable than those obtained with the blank sample. LOD was approximately 3.4 PFU/mL (Figs. S3 and S4). Moreover, a selectivity test was performed using the SARS-CoV-2 and influenza (pH1N1, H3N2, H5N2, and influenza B) viruses. The concentration of each virus was 10^2 PFU/mL. Data represent average ± standard deviation from 10

measurements. As shown in Fig. 5c, the intensity of the SERS signals significantly increased in the presence of SARS-CoV-2, however, weak signals were obtained in the presence of the influenza viruses. These data suggest that the developed SERS immunoassay can accurately detect the virus due to the high specificity of the selected antibody pair against SARS-CoV-2.

3.3. Diagnosis of COVID-19 patients

Nasopharyngeal swab samples have been primarily used for the diagnosis of COVID-19 because large numbers of respiratory epithelial cells, which are the initial sites for viral replication, can be aspirated from the nasopharyngeal tract (Gallo et al., 2021). Furthermore, the Centers for Disease Control and Prevention (CDC) recommended the use of nasopharyngeal swab samples for the initial diagnostic testing for SARS-CoV-2 infections (Centers for Disease Control and Prevention, 2021). Therefore, we tried to detect SARS-CoV-2 in human nasopharyngeal aspirates. The human nasal fluid samples were provided by the Yonsei University Health Service Center, Severance Hospital of Korea, after approval of the IRB. These samples tested negative for SARS-CoV-2. We intentionally spiked SARS-CoV-2 in the human nasopharyngeal aspirate samples and carried out the magnetically assisted SERS
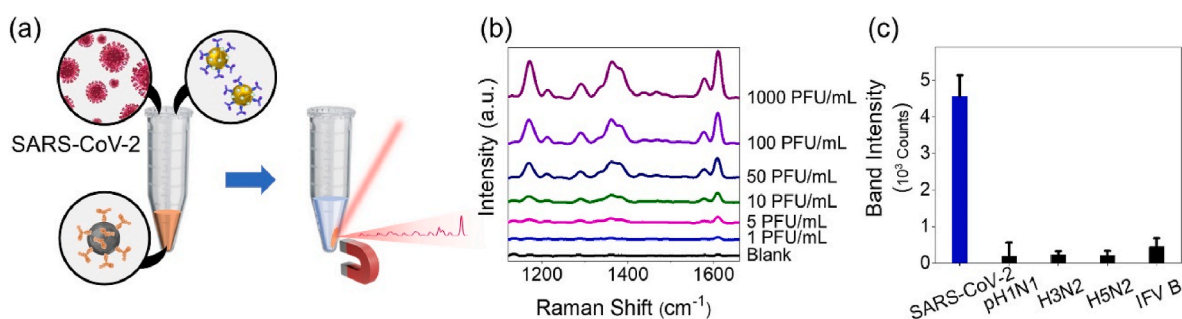

Fig. 5. (a) Schematic illustration of the magnetically assisted SERS immunoassay for SARS-CoV-2. (b) SERS spectra of MGITC measured using hollow Au NP-assembled magnetic beads after detection of SARS-CoV-2 (0–1000 PFU/mL). (c) A plot of 1170 cm^{-1} band intensity as a function of the virus. Data represent average ± standard deviation from 10 measurements.
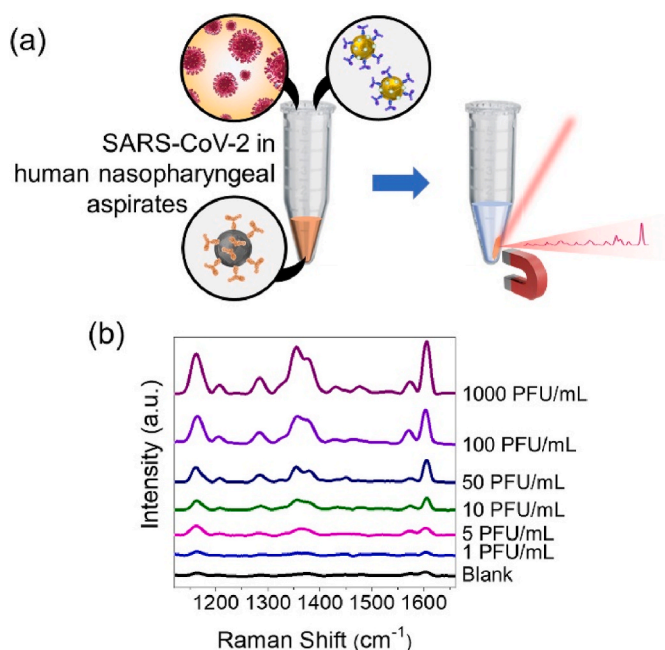
Fig. 6. (a) Schematic illustration of magnetically assisted SERS immunoassay for SARS-CoV-2-spiked human nasopharyngeal aspirate samples. (b) SERS spectra of MGITC measured from hollow Au NP-assembled magnetic beads after detection of SARS-CoV-2 (0–1000 PFU/mL) in human nasopharyngeal aspirate samples.

immunoassay. Figs. 6b and S5 show the results of the detection of SARS-CoV-2 in the human nasal fluid samples using the developed SERS method. Similar to the SARS-CoV-2 detection result in buffer (Fig. 5b), the SERS signals increased with the increasing concentration of SARS-CoV-2 in the nasal samples. However, the signals obtained from the blank samples were stronger and fluctuated compared with those shown in Fig. 5b. This is attributable to the non-specifically bound hollow Au NPs due to the presence of various components in human nasopharyngeal aspirates. Nevertheless, these data suggest that the current approach may facilitate the direct detection of SARS-CoV-2 in human nasopharyngeal swab samples. According to the previous results, the cyclic threshold (C_t) values of COVID-19 patients are mainly distributed in the range of 18.12–32.23 (mean of 27.16) (Azzi et al., 2020). Considering the relationship between C_t value and viral concentration (PFU/mL), the COVID-19 positive samples may include about 3000 PFU/mL of the virus (Chung et al., 2021). Because the present method can detect SARS-CoV-2 at lower concentrations than 3000 PFU/mL, we think the method has the potential for the diagnosis of COVID-19 patients.

Finally, we tried to diagnose COVID-19 patients using the magnetically assisted SERS immunoassay. Clinical samples from patients who tested positive for COVID-19 using PCR analysis were acquired from the Gyeongsang National University College of Medicine of Korea after IRB approval (Table S1). For the diagnosis, the clinical sample was incubated with the prepared magnetic beads and hollow Au NPs in a reaction tube for 25 min, and the resultant magnetic beads were collected using a magnet. In particular, we employed a portable Raman device to demonstrate the on-site diagnosis of COVID-19 patients (Fig. 7a). Therefore, the SERS signals of MGITC were observed from 15 clinical samples of COVID-19 patients (blue spectra in Fig. 7b). Furthermore, weak signals were observed from four negative control samples (black spectra in Fig. 7b). The plot of 1170 cm^{-1} band intensity versus clinical sample shows the positively and negatively diagnosed results (Fig. 7c). Data represent average $\pm$ standard deviation from 3 measurements. These data suggest that the present method can be employed for the on-site diagnosis of COVID-19 patients, and this is the first SERS-based
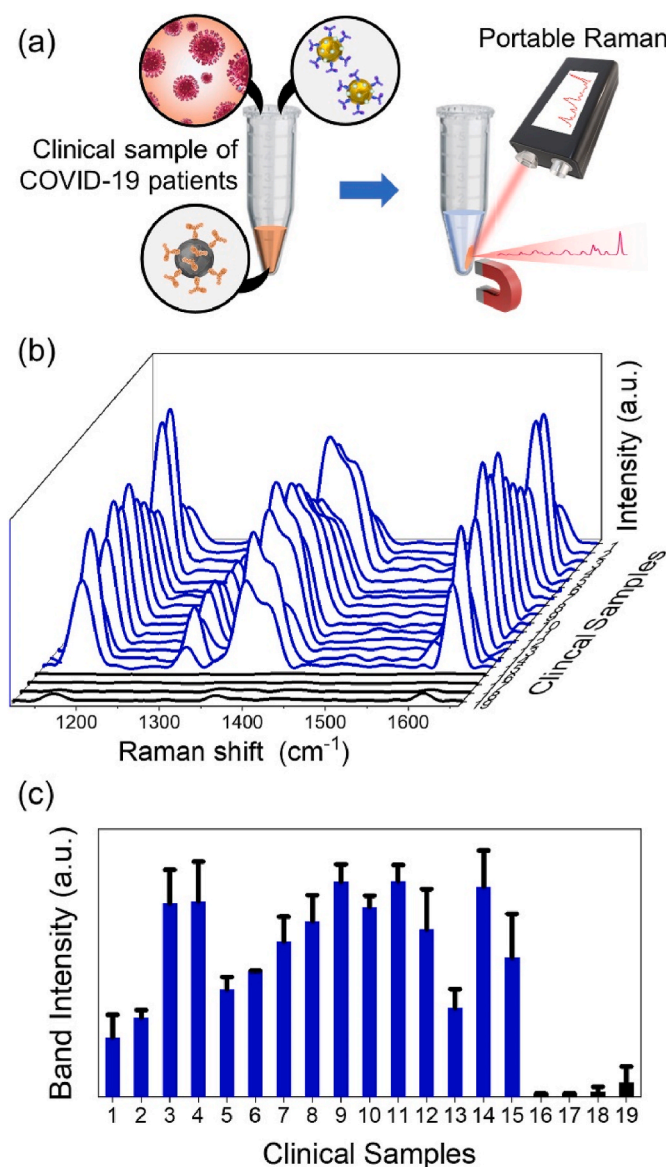

Fig. 7. (a) Schematic illustration of the magnetically assisted SERS immunoassay using a portable Raman device for clinical samples obtained from COVID-19 patients. (b) SERS spectra of MGITC measured from hollow Au NP-assembled magnetic beads after the diagnosis of COVID-19 patients. (c) A plot of 1170 cm^{-1} band intensity as a function of clinical samples. Samples 1–15 were obtained from patients positively diagnosed for COVID-19, whereas samples 16–19 were from the negatively diagnosed patients. Data represent average $\pm$ standard deviation from three measurements.

assay for the detection of SARS-CoV-2 in COVID-19 patients. The simplicity of the developed assay and the use of a portable Raman device enabled the successful diagnosis of the patients. Based on these data, we hope to widen the practical applications of SERS-based assays for the detection of infectious viruses.

4. Discussion

PCR-based techniques have high sensitivity and specificity and have thus been primarily used for the diagnosis of COVID-19 patients at various centralized laboratories (Huang et al., 2020; Vogels et al., 2020). Complementary point-of-care (POC) diagnostic tests, such as antigen tests, are cost-efficient and have thus been used to rapidly detect SARS-CoV-2 and prevent its transmission (Collier et al., 2020; Raziq et al., 2021). For the development of antigen tests, high-performance

antibodies against the target antigens are critical. Thus, we developed two monoclonal antibodies having high affinity and specificity for the SARS-CoV-2 antigen. These antibodies are suitable for the detection of the virus using sandwich ELISA, enabling the successful identification of SARS-CoV-2 through a SERS-based assay. COVID-19 is predicted to become an endemic disease (Torjesen, 2021; Veldhoen and Simas, 2021); therefore, the development of multiplex POC devices is crucial to distinguish different respiratory illnesses in the future (Veldhoen and Simas, 2021). Our group has been involved in successfully developing various types of antibodies for the detection of viruses to date (Kim et al., 2021; Orooji et al., 2021). Thus, in the near future, we plan to combine such high-performance antibodies to develop a multiplex immunoassay for infectious viruses.

The LOD of the current method is over 10 times lower than that of the commercially available SARS-CoV-2 antigen diagnostic kits (Table S2). Furthermore, the LOD is quite impressive compared with that of the previously reported state-of-the-art SARS-CoV-2 antigen detection methods (Table S3). This high sensitivity may be due to the synergistic combination of the high-performance antibody pair and high-quality SERS-active hollow Au NPs. In particular, hollow Au NPs show strong enhancement effects from individual particles because of their ability to localize the surface electromagnetic fields through the pinholes in the hollow particle structures. We compared SERS signals of hollow Au NP and commercially available Au NPs after the detection of SARS-CoV-2 antigen, confirming the strong enhancement effect of hollow Au NPs (Fig. S6).

There have been several recent advances in antigen tests, involving the application of various sensing approaches and high-quality nanomaterials (Cennamo et al., 2021; Eissa et al., 2021; Grant et al., 2020; Huang et al., 2021; Lin et al., 2020; Seo et al., 2020). SERS is an effective technique for the sensitive detection of biomolecules, and various SERS-based immunoassays have thus been developed for the detection of infectious viruses (Saviñon-Flores et al., 2021). Following the emergence of the COVID-19 pandemic, several SERS-based methods for SARS-CoV-2 have been applied (Zhang et al., 2021; Wu et al., 2022; Yang et al., 2021; Yu et al., 2021; Srivastav et al., 2021; Sanchez et al., 2021; Payne et al., 2021; Liu et al., 2021; Li et al., 2021; Huang et al., 2021; Gao et al., 2021; Chen et al., 2021; Chen et al., 2021, 2021; Huang et al., 2021, 2021; Pramanik et al., 2021; Zavyalova et al., 2021). However, the current magnetically assisted SERS immunoassay is the only assay developed so far that facilitates the on-site diagnosis of the samples of COVID-19 patients. Using a portable Raman device, we can accurately distinguish the SARS-CoV-2 positive and negative clinical samples. Furthermore, these tests can be performed within 30 min, suggesting that the method can be applied for POC testing for COVID-19.

Recently, several types of sensing approaches have been employed for the diagnosis, screening, and surveillance of SARS-CoV-2 (Cennamo et al., 2021; Chen et al., 2021; Corman et al., 2020; Eissa et al., 2021; Grant et al., 2020; Huang et al., 2020, 2021; Kevadiya et al., 2021; Lin et al., 2020; Liu et al., 2021; Mina and Andersen, 2021; Moon et al., 2020; Peng et al., 2021a,b; Seo et al., 2020; Shi and Ren, 2021; Wang et al., 2020; Yang et al., 2021; Zhang et al., 2020, 2021). The current SERS immunoassay may be useful for entry screening to detect infected individuals before allowing access to facilities, such as schools, because COVID-19 leads to a substantially reduced mortality in children and young students (Kevadiya et al., 2021; Mina and Andersen, 2021). A previous study reported that, of the 72,500 samples collected from asymptomatic individuals, 1405 were found to be positive for SARS-CoV-2 at the University of Colorado, Boulder (Álvarez-Díaz et al., 2020). This report restates the necessity of entry screening for SARS-CoV-2 to prevent the spread of the virus in schools. Recently, entry screening has been conducted at the Seoul National University of Korea before allowing students access to face-to-face lectures. Although wearing a mask and physical distancing should be practiced even after a negative screening test result, we anticipate that such efforts to develop advanced diagnostic methods for COVID-19 will enable a safer society in the near future.

Despite all the advantages of the present method, there is room for improvement. Considering the daily tested numbers for COVID-19, an automated system for massive analysis of samples is required. Moreover, the synthesis of hollow Au NPs and antibodies on a large scale should be a precedence for practical application. Although we demonstrated the detection of SARS-CoV-2 using a portable Raman device, precise optimization and comparison with a gold standard assay should be performed. We are continuing to study SERS-based viral detection techniques for the diagnosis of emerging infectious diseases.

5. Conclusions

Herein, we reported a SERS-based immunoassay for SARS-CoV-2 using a developed antibody pair, hollow Au NPs, and magnetic beads. The assay could detect the SARS-CoV-2 antigen at a low concentration of 2.56 fg/mL and the viral lysates at 3.4 PFU/mL. Furthermore, it facilitated the identification of SARS-CoV-2 in human nasopharyngeal aspirates. Most importantly, we successfully diagnosed COVID-19 patients within 30 min using a portable Raman system, demonstrating the potential of the current assay for the diagnosis and prevention of SARS-CoV-2.

CRediT authorship contribution statement

Hyunjung Cha: Methodology, Validation, Investigation, Data curation, Writing – original draft. **Hyeran Kim:** Methodology, Validation, Formal analysis, Investigation, Resources, Data curation. **Younju Joung:** Investigation, Resources, Writing – review & editing. **Hyunju Kang:** Investigation, Writing – review & editing. **Jeong Moon:** Investigation. **Hyowon Jang:** Investigation. **Sohyun Park:** Resources. **Hyung-Jun Kwon:** Resources. **In-Chul Lee:** Resources. **Sunjoo Kim:** Resources. **Dongeun Yong:** Resources. **Sun-Woo Yoon:** Resources. **Sung-Gyu Park:** Resources. **Kyeonghye Guk:** Resources. **Eun-Kyung Lim:** Investigation, Funding acquisition. **Hyun Gyu Park:** Investigation. **Jaebum Choo:** Resources, Writing – review & editing, Funding acquisition. **Juyeon Jung:** Investigation, Resources, Supervision, Funding acquisition. **Taejoon Kang:** Conceptualization, Methodology, Validation, Formal analysis, Investigation, Resources, Data curation, Writing – original draft, Writing – review & editing, Visualization, Supervision, Project administration, Funding acquisition.

Declaration of competing interest

The authors declare that they have no known competing financial interests or personal relationships that could have appeared to influence the work reported in this paper.

Appendix A. Supplementary data

Supplementary data to this article can be found online at https://doi.org/10.1016/j.bios.2022.114008.

References

Álvarez-Díaz, D.A., Franco-Muñoz, C., Laiton-Donato, K., Usme-Ciro, J.A., Franco-Sierra, N.D., Flórez-Sánchez, A.C., Gómez-Rangel, S., Rodríguez-Calderon, L.D., Barbosa-Ramirez, J., Ospitia-Baez, E., Walteros, D.M., Ospina-Martinez, M.L., Mercado-Reyes, M., 2020. Infect. Genet. Evol. 84, 104390.

Azzi, L., Carcano, G., Gianfagna, F., Grossi, P., Dalla Gasperina, D., Genoni, A., Baj, A., 2020. J. Infect. 81, e45–e50.

Cennamo, N., D'Agostino, G., Perri, C., Arcadio, F., Chiaretti, G., Parisio, E.M., Camarlinghi, G., Vettori, C., Di Marzo, F., Cennamo, R., Porto, G., Zeni, L., 2021. Sensors 21, 1681.

Centers for Disease Control and Prevention, 2021. https://www.cdc.gov/coronavirus/2019-ncov/lab/guidelines-clinical-specimens.html.

Chen, H., Park, S.G., Choi, N., Kwon, H.J., Kang, T., Lee, M.K., Choo, J., 2021. ACS Sens. 6, 2378–2385.

Chen, S., Meng, L., Wang, L., Huang, X., Ali, S., Chen, X., Yu, M., Yi, M., Li, L., Chen, X., Yuan, L., Shi, W., Huang, G., 2021. Sensor. Actuator. B 348, 130706.

Choi, N., Dang, H., Das, A., Sim, M.S., Chung, I.Y., Choo, J., 2020. Biosens. Bioelectron. 164, 112326.

Chung, Y.S., Lee, N.J., Woo, S.H., Kim, J.M., Kim, H.M., Jo, H.J., Park, Y.E., Han, M.G., 2021. Sci. Rep. 11, 14817.

Collier, D.A., Assennato, S.M., Warne, B., Sithole, N., Sharrocks, K., Ritchie, A., Ravji, P., Routledge, M., Sparkes, D., Skittrall, J., Smielewska, A., 2020. Cell Rep. Med. 1, 100062.

Corman, V.M., Landt, O., Kaiser, M., Molenkamp, R., Meijer, A., Chu, D.K., Bleicker, T., Brünink, S., Schneider, J., Schmidt, M.L., Mulders, D.G., Haagmans, B.L., van der Veer, B., van den Brink, S., Wijsman, L., Goderski, G., Romette, J.L., Ellis, J., Zambon, M., Peiris, M., Goossens, H., Reusken, C., Koopmans, M.P., Drosten, C., 2020. Euro Surveill. 25, 2001035.

Eissa, S., Alhadrami, H.A., Al-Mozaini, M., Hassan, A.M., Zourob, M., 2021. Mikrochim. Acta 188, 199.

Eom, G., Hwang, A., Kim, H., Yang, S., Lee, D.K., Song, S., Ha, K., Jeong, J., Jung, J., Lim, E.K., Kang, T., 2019a. ACS Sens. 4, 2282–2287.

Eom, G., Hwang, A., Lee, D.K., Guk, K., Moon, J., Jeong, J., Jung, J., Kim, B., Lim, E.K., Kang, T., 2019b. ACS Appl. Bio Mater. 1233–1240.

Forthal, D.N., 2014. Microbiol. Spectr. 2, 1–17.

Gallo, O., Locatello, L.G., Mazzoni, A., Novelli, L., Annunziato, F., 2021. Mucosal Immunol. 14, 305–316.

Gao, Y., Han, Y., Wang, C., Qiang, L., Gao, J., Wang, Y., Liu, H., Han, L., Zhang, Y., 2021. Anal. Chim. Acta 1154, 338330.

Grant, B.D., Anderson, C.E., Williford, J.R., Alonzo, L.F., Glukhova, V.A., Boyle, D.S., Weigl, B.H., Nichols, K.P., 2020. Anal. Chem. 92, 11305–11309.

Guk, K., Kim, H., Lee, M., Choi, Y.A., Hwang, S.G., Han, G., Kim, H.N., Kim, H., Park, H., Yong, D., Kang, T., Lim, E.K., Jung, J., 2020. Nat. Commun. 11, 3418.

Guo, J., Chen, Y., Jiang, Y., Ju, H., 2017. Chemistry 23, 9332–9337.

Huang, G., Zhao, H., Li, P., Liu, J., Che, S., Ge, M., Qin, M., Zhou, G., Wang, Y., Li, S., Cheng, Y., Huang, Q., Wang, J., Wang, H., Yang, L., 2021. Anal. Chem. 93, 16086–16095.

Huang, J., Wen, J., Zhou, M., Ni, S., Le, W., Chen, G., Wei, L., Zeng, Y., Qi, D., Pan, M., Xu, J., Wu, Y., Li, Z., Feng, Y., Zhao, Z., He, Z., Li, B., Zhao, S., Zhang, B., Xue, P., He, S., Fang, K., Zhao, Y., Du, K., 2021. Anal. Chem. 93, 9174–9182.

Huang, L., Ding, L., Zhou, J., Chen, S., Chen, F., Zhao, C., Xu, J., Hu, W., Ji, J., Xu, H., Liu, G.L., 2021. Biosens. Bioelectron. 171, 112685.

Huang, W.E., Lim, B., Hsu, C.C., Xiong, D., Wu, W., Yu, Y., Jia, H., Wang, Y., Zeng, Y., Ji, M., Chang, H., Zhang, X., Wang, H., Cui, Z., 2020. Microb. Biotechnol. 13, 950–961.

Hwang, A., Kim, E., Moon, J., Lee, H., Lee, M., Jeong, J., Lim, E.K., Jung, J., Kang, T., Kim, B., 2019. ACS Appl. Mater. Interfaces 11, 18960–18967.

Kahraman, M., Mullen, E.R., Korkmaz, A., Wachsmann-Hogiu, S., 2017. Nanophotonics 6, 831–852.

Kamińska, A., Winkler, K., Kowalska, A., Witkowska, E., Szymborski, T., Janeczek, A., Waluk, J., 2017. Sci. Rep. 7, 10656.

Kang, T., Yoo, S.M., Yoon, I., Lee, S.Y., Kim, B., 2010. Nano Lett. 10, 1189–1193.

Kevadiya, B.D., Machhi, J., Herskovitz, J., Oleynikov, M.D., Blomberg, W.R., Bajwa, N., Soni, D., Das, S., Hasan, M., Patel, M., Senan, A.M., Gorantla, S., McMillan, J., Edagwa, B., Eisenberg, R., Gurumurthy, C.B., Reid, S.P.M., Punyadeera, C., Chang, L., Gendelman, H.E., 2021. Nat. Mater. 20, 593–605.

Khan, M.I., Khan, Z.A., Baig, M.H., Ahmad, I., Farouk, A.E., Song, Y.G., Dong, J.J., 2020. PLoS One 15, e0238344.

Kim, H., Kang, H., Kim, H.N., Kim, H., Moon, J., Guk, K., Park, H., Yong, D., Bae, P.K., Park, H.G., Lim, E.K., 2021. Biosens. Bioelectron. 187, 113324.

Li, J., Wuethrich, A., Edwardraja, S., Lobb, R.J., Puttick, S., Rose, S., Howard, C.B., Trau, M., 2021. Anal. Chem. 93, 10251–10260.

Lin, Q., Wen, D., Wu, J., Liu, L., Wu, W., Fang, X., Kong, J., 2020. Anal. Chem. 92, 9454–9458.

Liu, H., Dai, E., Xiao, R., Zhou, Z., Zhang, M., Bai, Z., Shao, Y., Qi, K., Tu, J., Wang, C., Wang, S., 2021. Sensor. Actuator. B Chem. 329, 129196.

Lu, R., Zhao, X., Li, J., Niu, P., Yang, B., Wu, H., Wang, W., Song, H., Huang, B., Zhu, N., Bi, Y., Ma, X., Zhan, F., Wang, L., Hu, T., Zhou, H., Hu, Z., Zhou, W., Zhao, L., Chen, J., Meng, Y., Wang, J., Lin, Y., Yuan, J., Xie, Z., Ma, J., Liu, W.J., Wang, D., Xu, W., Holmes, E.C., Gao, G.F., Wu, G., Chen, W., Shi, W., Tan, W., 2020. Lancet 395, 565–574.

Mahmuda, A., Bande, F., Al-Zihiry, K.J.K., Abdulhaleem, N., Abd Majid, R., Hamat, R.A., Abdullah, W.O., Unyah, Z., 2017. Trop. J. Pharmaceut. Res. 16, 713.

Mina, M.J., Andersen, K.G., 2021. Science 371, 126–127.

Moon, J., Kwon, H.J., Yong, D., Lee, I.C., Kim, H., Kang, H., Lim, E.K., Lee, K.S., Jung, J., Park, H.G., Kang, T., 2020. ACS Sens. 5, 4017–4026.

Orooji, Y., Sohrabi, H., Hemmat, N., Oroojalian, F., Baradaran, B., Mokhtarzadeh, A., Mohaghegh, M., Karimi-Maleh, H., 2021. Nano-Micro Lett. 13, 18.

Payne, T.D., Klawa, S.J., Jian, T., Kim, S.H., Papanikolas, M.J., Freeman, R., Schultz, Z. D., 2021. ACS Sens. 6, 3436–3444.

Peng, Y., Lin, C., Long, L., Masaki, T., Tang, M., Yang, L., Liu, J., Huang, Z., Li, Z., Luo, X., Lombardi, J.R., Yang, Y., 2021a. Nano-Micro Lett. 13, 52.

Peng, Y., Lin, C., Li, Y., Gao, Y., Wang, J., He, J., Huang, Z., Liu, J., Luo, X., Yang, Y., 2021b. Matter ASAP.

Pramanik, A., Gao, Y., Patibandla, S., Mitra, D., McCandless, M.G., Fassero, L.A., Gates, K., Tandon, R., Ray, P.C., 2021. Nanoscale Adv. 3, 1588–1596.

Raziq, A., Kidakova, A., Boroznjak, R., Reut, J., Öpik, A., Syritski, V., 2021. Biosens. Bioelectron. 178, 113029.

Richman, D.D., 2021. Glob. Health Med. 3, 1–5.

Sanchez, J.E., Jaramillo, S.A., Settles, E., Salazar, J.J.V., Lehr, A., Gonzalez, J., Aranda, C.R., Navarro-Contreras, H.R., Raniere, M.O., Harvey, M., Wagner, D.M., Koppisch, A., Kellar, R., Keim, P., Yacaman, M.J., 2021. RSC Adv. 11, 25788–25794.

Saviñon-Flores, F., Méndez, E., López-Castaños, M., Carabarin-Lima, A., López-Castaños, K.A., González-Fuentes, M.A., Méndez-Albores, A., 2021. Biosensors 11, 66.

Schechinger, M., Marks, H., Mabbott, S., Choudhury, M., Cote, G., 2019. Analyst 144, 4033–4044.

Seo, G., Lee, G., Kim, M.J., Baek, S.H., Choi, M., Ku, K.B., Lee, C.S., Jun, S., Park, D., Kim, H.G., Kim, S.J., Lee, J.O., Kim, B.T., Park, E.C., Kim, S.I., 2020. ACS Nano 14, 5135–5142.

Shi, A.C., Ren, P., 2021. J. Immunol. Methods 494, 113060.

Shin, H., Jeong, H., Park, J., Hong, S., Choi, Y., 2018. ACS Sens. 3, 2637–2643.

Srivastav, S., Dankov, A., Adanalic, M., Grzeschik, R., Tran, V., Pagel-Wieder, S., Gessler, F., Spreitzer, I., Scholz, T., Schnierle, B., Anastasiou, O.E., Dittmer, U., Schlücker, S., 2021. Anal. Chem. 93, 12391–12399.

Sun, Y., Xu, L., Zhang, F., Song, Z., Hu, Y., Ji, Y., Shen, J., Li, B., Lu, H., Yang, H., 2017. Biosens. Bioelectron. 89, 906–912.

Torjesen, I., 2021. BMJ 372, n494.

Veldhoen, M., Simas, J.P., 2021. Nat. Rev. Immunol. 21, 131–132.

Vogels, C.B., Brito, A.F., Wyllie, A.L., Fauver, J.R., Ott, I.M., Kalinich, C.C., Petrone, M.E., Casanovas-Massana, A., Muenker, M.C., Moore, A.J., Klein, J., 2020. Nat. Microbiol. 5, 1299–1305.

Wang, M., Fu, A., Hu, B., Tong, Y., Liu, R., Liu, Z., Gu, J., Xiang, B., Liu, J., Jiang, W., Shen, G., Zhao, W., Men, D., Deng, Z., Yu, L., Wei, W., Li, Y., Liu, T., 2020. Small 16, e2002169.

World Health Organization, 2021. https://covid19.who.int/.

Wu, Y., Dang, H., Park, S.G., Chen, L., Choo, J., 2022. Biosens. Bioelectron. 197, 113736.

Yadav, S., Senapati, S., Desai, D., Gahlaut, S., Kulkarni, S., Singh, J.P., 2021. Colloids Surf. B Biointerfaces 198, 111477.

Yang, Q., Saldi, T.K., Gonzales, P.K., Lasda, E., Decker, C.J., Tat, K.L., Fink, M.R., Hager, C.R., Davis, J.C., Ozeroff, C.D., Muhlrad, D., Clark, S.K., Fattor, W.T., Meyerson, N.R., Paige, C.L., Gilchrist, A.R., Barbachano-Guerrero, A., Worden-Sapper, E.R., Wu, S.S., Brisson, G.R., McQueen, M.B., Dowell, R.D., Leinwand, L., Parker, R., Sawyer, S.L., 2021. Proc. Natl. Acad. Sci. U. S. A. 118, e2104547118.

Yang, Y., Pen, Y., Lin, C., Long, L., Hu, J., He, J., Zeng, H., Huang, Z., Li, Z.Y., Tanemura, M., Shi, J., Lombardi, J.R., Luo, X., 2021. Nano-Micro Lett. 13, 109.

Yu, Q., Wu, Y., Kang, T., Choo, J., 2021. Bull. Kor. Chem. Soc. 42, 1699–1705.

Zavyalova, E., Ambartsumyan, O., Zhdanov, G., Gribanyov, D., Gushchin, V., Tkachuk, A., Rudakova, E., Nikiforova, M., Kuznetsova, N., Popova, L., Verdiev, B., Alatyrev, A., Burtseva, E., Ignatieva, A., Iliukhina, A., Dolzhikova, I., Arutyunyan, A., Gambaryan, A., Kukushkin, V., 2021. Nanomaterials 11, 1394.

Zhang, C., Zhou, L., Du, K., Zhang, Y., Wang, J., Chen, L., Lyu, Y., Li, J., Liu, H., Huo, J., Li, F., Wang, J., Sang, P., Lin, S., Xiao, Y., Zhang, K., He, K., 2020. Front. Cell. Infect. Microbiol. 10, 553837.

Zhang, D., Zhang, X., Ma, R., Deng, S., Wang, X., Wang, X., Zhang, X., Huang, X., Liu, Y., Li, G., Qu, J., Zhu, Y., Li, J., 2021. Water Res. 200, 117243.